Article

Pre-Season Precipitation and Temperature Have a Larger Influence on Vegetation Productivity than That of the Growing Season in the Agro-Pastoral Ecotone in Northern China

Yuanyuan Zhang [1,2], Qingtao Wang [1,*], Xueyuan Zhang [3,4], Zecheng Guo [5], Xiaonan Guo [6], Changhui Ma [2], Baocheng Wei [7] and Lei He [2,3]

1 School of Landscape and Ecological Engineering, Hebei University of Engineering, Handan 056000, China; yuanmu198@gmail.com
2 State Key Laboratory of Efficient Utilization of Arid and Semi-arid Arable Land in Northern China, Institute of Agricultural Resources and Regional Planning, Chinese Academy of Agricultural Sciences, Beijing 100081, China; machanghui@caas.cn (C.M.); helei@caas.cn (L.H.)
3 College of Earth and Environmental Sciences, Lanzhou University, Lanzhou 730000, China; zhangxueyuan21@lzu.edu.cn
4 School of Design and the Built Environment, Curtin University, Bentley 6102, Australia
5 Faculty of Geomatics, Lanzhou Jiaotong University, Lanzhou 730000, China; guozecheng@lzjtu.edu.cn
6 School of Land Science and Space Planning, Hebei International Joint Research Center for Remote Sensing of Agricultural Drought Monitoring, Hebei GEO University, Shijiazhuang 050031, China; guoxiaonan@hgu.edu.cn
7 College of Geographical Science, Inner Mongolia Normal University, Hohhot 010022, China; nsdwbc@imnu.edu.cn
* Correspondence: wangqingtao@hebeu.edu.cn

Abstract: Climate change and human activities are reshaping the structure and function of terrestrial ecosystems, particularly in vulnerable regions such as agro-pastoral ecotones. However, the extent to which climate change impacts vegetation growth in these areas remains poorly understood, largely due to the modifying effects of human-induced land cover changes on vegetation sensitivity to climatic variations. This study utilizes satellite-derived vegetation indices, land cover datasets, and climate data to investigate the influence of both land cover and climate changes on vegetation growth in the agro-pastoral ecotone of northern China (APENC) from 2001 to 2022. The results reveal that the sensitivity of vegetation productivity, as indicated by the kernel Normalized Difference Vegetation Index (kNDVI), varies depending on the land cover type to climate change in the APENC. Moreover, ridge regression modeling shows that pre-season climate conditions (i.e., pre-season precipitation and temperature) have a stronger positive impact on growing-season vegetation productivity than growing season precipitation and temperature, while the effect of vapor pressure deficit (VPD) is negative. Notably, the kNDVI exhibits significant positive sensitivity ($p < 0.05$) to precipitation in 34.12% of the region and significant negative sensitivity ($p < 0.05$) to VPD in 38.80%. The ridge regression model explained 89.10% of the total variation ($R^2 = 0.891$). These findings not only emphasize the critical role of both historical and contemporary climate conditions in shaping vegetation growth but also provide valuable insights into how to adjust agricultural and animal husbandry management strategies to improve regional climate adaptation based on climate information from previous seasons in fragile regions.

Keywords: vegetation productivity; climate change; land cover change; precipitation patterns; pre-season climate; APENC

1. Introduction

Terrestrial ecosystems are increasingly affected by anthropogenic climate change (e.g., global warming and accelerated hydrological cycles) and human-dominated land use/land cover changes (LUCC), such as urbanization, deforestation, afforestation, and agricultural expansion [1–3]. In response to these stressors, terrestrial ecosystems adapt by altering their structural composition and modifying their sensitivity to climatic variations, consequently influencing ecosystem functions, particularly primary productivity [3,4]. Therefore, understanding the impacts of climate change and LUCC on vegetation primary productivity is essential for effective ecological resource management and ensuring human well-being, particularly in regions heavily dependent on primary productivity for food, fuel, and fiber.

The arid and semi-arid agricultural pastoral ecotone of northern China (hereafter the APENC), a transition zone between agricultural cultivation and animal husbandry, is a typical fragile ecological zone that is highly vulnerable to climate change due to frequent human-dominated LUCC [5]. Historically, the extensive conversion of grasslands and forestlands into croplands between the 1960s and 1990s led to severe ecological degradation, including reduced ecological functionality, land degradation, and increased soil erosion [6]. To address these issues, several ecological projects, such as the "Three-North Shelterbelt", "Grain for Green", and "Beijing-Tianjin Sand-Storm Source" projects, have been implemented since 1999, significantly altering the LUCC dynamics in the APENC [7]. These land cover changes have induced local biome shifts, potentially modifying the sensitivity of vegetation to climatic factors, including temperature increases, precipitation variability, and rising vapor pressure deficit (VPD) [8]. However, the extent to which frequent transitions between grassland and cropland affect the sensitivity of vegetation to climate changes remains poorly understood, thereby limiting a comprehensive understanding of vegetation–climate interactions.

In addition to the impacts of LUCC, the APENC is highly sensitive to climate change [9]. Precipitation, a primary limiting factor in dryland ecosystems, plays a critical role in shaping vegetation productivity in the region [10]. Unlike temperature, precipitation variability encompasses multiple dimensions, including changes in total amount, intensity, and frequency, each exerting distinct influences on vegetation productivity through various mechanisms [11]. However, existing research has predominantly focused on the effects of the total precipitation amount, neglecting variations in precipitation intensity and frequency. For instance, Xue et al. [12] identified total precipitation as the primary determinant of vegetation greenness, a proxy for productivity, in the APENC. Similarly, Liu et al. [13] and Chen et al. [14] employed cumulative precipitation amounts to study vegetation response to climate changes. Such studies, while insightful, offer an incomplete understanding of the complex interactions between precipitation regimes and vegetation productivity, leading to oversimplified assessments of climate impacts.

Among the various climatic factors, pre-season temperature and precipitation played critical roles in regulating plant growth, particularly in arid and semi-arid regions [15,16]. Previous studies showed that snow cover played a critical role by regulating soil moisture, temperature, and nutrient dynamics, which in turn influenced plant growth and ecosystem productivity [17,18]. According to Yang et al. [19], the impact of winter snowfall on vegetation persisted into the growing season. Huang et al. [20] noted that excess moisture from more snowfall promoted vegetation growth at elevations lower than 3000 m. However, at elevations higher than 3000 m, more snowfall delayed the onset of spring and inhibited plant growth [20]. Similarly, pre-season conditions influenced vegetation activity—warmer temperatures triggered early growth, while colder temperatures delayed it [21]. These findings underscored the importance of understanding pre-season climatic conditions as

they directly shaped plant growth dynamics and overall ecosystem productivity in regions sensitive to climate variability.

In the context of climate–vegetation interactions, analyzing the sensitivity of vegetation productivity to climatic variables is essential for understanding ecosystem responses to climate change [22]. However, the complex relationships among multiple climatic factors often result in multicollinearity, which can distort the outcomes of traditional regression-based methods [8]. To overcome this issue, this study employs ridge regression, a robust statistical technique specifically designed to address multicollinearity by applying L2 regularization to stabilize the model coefficients [23]. This approach effectively mitigates the influence of correlated predictors, resulting in more reliable and interpretable results. In addition, ridge regression not only enhances the precision of parameter estimates but also improves the overall robustness of the model, making it particularly suitable for complex, high-dimensional data like climate–vegetation interactions [24].

This study aims to address two key research questions:

(1) Is the sensitivity of vegetation productivity to climate variables (including VPD and precipitation) affected by LUCC in the APENC region?
(2) How do precipitation metric interactions and vegetation productivity respond to the sensitivity of vegetation in the APENC?

To explore these questions, the study utilizes the recently developed kernel Normalized Difference Vegetation Index (kNDVI), which offers an improved representation of Gross Primary Productivity across diverse biomes [25]. Additionally, the study integrates data from land cover dataset and multi-source merged climate records to analyze vegetation responses to climate change in the APENC from 2001 to 2022.

2. Materials and Methods

2.1. Study Area

The agro-pastoral ecotone of northern China (APENC) is located in the northern region of the Loess Plateau and the southeastern part of the Mongolian Plateau, spanning latitudes 33.5–48.6° N and longitudes 101–126.5° E. The region covers approximately 835,000 km^2 and extends across 11 provinces and autonomous regions, including Inner Mongolia, Heilongjiang, Jilin, Liaoning, Beijing, Hebei, Shanxi, Shaanxi, Ningxia, Gansu, and Qinghai (Figure 1a) [26]. APENC is characterized by an arid to semi-arid climate, with mean annual temperatures ranging from 2 °C to 8 °C and mean annual precipitation between 300 mm and 450 mm. Notably, approximately 60% to 70% of the total annual precipitation occurs during the summer months (June to August). The dominant vegetation types exhibit a gradual transition from forest and forest steppe in the northeast to typical steppe and desert steppe in the southwest [27].
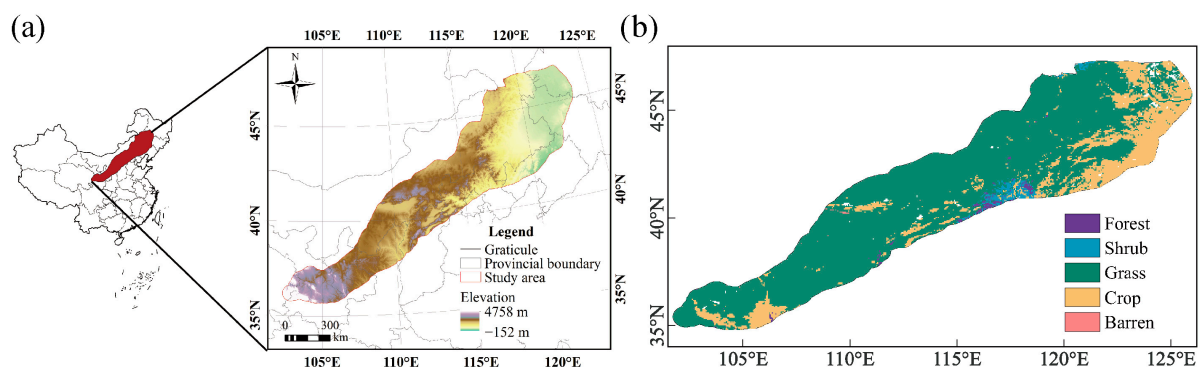

Figure 1. Maps of study area. (**a**) Location and elevation of the agro-pastoral ecotone of northern China (APENC). (**b**) Land use and land cover types of APENC in 2022.

2.2. Datasets

2.2.1. Vegetation Productivity

In the selection of vegetation indices (VIs), NDVI (Normalized Difference Vegetation Index), EVI (Enhanced Vegetation Index), and GPP (Gross Primary Productivity) are widely used to assess vegetation productivity but face notable limitations. NDVI suffers from saturation effects in areas with high vegetation density [28], while EVI, though reducing this issue with additional spectral bands, still struggles with accuracy under such conditions [29]. GPP, a direct measure of photosynthetic activity, relies on solar-induced chlorophyll fluorescence (SIF) for improved precision but is constrained by incomplete SIF–GPP relationships and limited spatial and temporal resolution [30,31].

In contrast, kNDVI employs higher-order statistical relationships among spectral reflectances to effectively address saturation issues in NDVI and EVI. This kernel–based approach ensures robust and accurate vegetation productivity assessments across diverse phenological cycles and climatic zones. Furthermore, kNDVI's strong correlation with GPP and SIF enhances its capability to capture photosynthetic activity, making it a more reliable and versatile index for applications such as crop yield estimation and environmental monitoring [28]. kNDVI is calculated as $\text{kNDVI} = \tanh(\text{NDVI}^2)$ [28], offering a more reliable measure of vegetation productivity. For this study, the kernel Normalized Difference Vegetation Index (kNDVI) was derived from the Moderate Resolution Imaging Spectroradiometer (MODIS) MOD13C2 v061 product, which has a monthly temporal resolution and a spatial resolution of 0.05°. MODIS, a NASA instrument, collects comprehensive data on the Earth's surface, land, oceans, and atmosphere. This data is invaluable for studying global processes and dynamics and plays a crucial role in climate change prediction and environmental monitoring. Publicly available datasets were analyzed in this study. These data can be found here: [https://lpdaac.usgs.gov/products/mod13c2v061/], accessed on 1 October 2023. The analysis covered the period from 2001 to 2022, allowing for the assessment of long–term vegetation trends.

2.2.2. Land Cover Dataset

Annual land cover data were obtained from the MODIS MCD12C1 product, which provides a spatial resolution of 0.05° [32]. Publicly available datasets were analyzed in this study. These data can be found here: [https://lpdaac.usgs.gov/products/mcd12c1v006/], accessed on 1 October 2023. The land cover types classified by the International Geosphere–Biosphere Programme (IGBP) were consolidated into five categories for APENC: forestland, shrubland, grassland, cropland, and barren land (Figure 1b).

2.2.3. Climate Data

Daily climate data with a spatial resolution of 0.1° were sourced from the Multi–Source Weighted Ensemble Precipitation (MSWEP) dataset [33]. Publicly available datasets were analyzed in this study. These data can be found here: [https://www.gloh2o.org/mswep/], accessed on 1 October 2023. Considering both the temporal dynamics of precipitation regimes and their time–lag effects, the following precipitation metrics were calculated for the growing season (April to October): total precipitation amount, precipitation intensity, precipitation frequency, and dry–day fraction. In addition, pre–season precipitation (November of the previous year to March of the current year) was also assessed. Precipitation intensity (P_{int}) was determined as the ratio of the total precipitation amount to wet days (daily precipitation ≥ 0.1 mm) during growing –season [34]. The ratio of the number of dry days (daily precipitation < 0.1 mm) to the total number of growing–season days was used to compute dry–day fraction (f_{dry}) [34]. The Unranked–Gini index (UGi), which

describes how the precipitation amount is irregularly distributed, was employed to indicate precipitation frequency (P_{fre}) [34].

In addition to precipitation metrics, other climatic variables were incorporated, including mean temperature, mean radiation, and mean VPD during the growing season, as well as pre–season mean temperature. These variables were derived from the Multi–Source Weather (MSWX) dataset [35]. Publicly available datasets were analyzed in this study. These data can be found here: [https://www.gloh2o.org/mswx/], accessed on 1 October 2023. VPD was calculated using the "plantecophys" package in R, based on air temperature, relative humidity, and air pressure [36]. Additionally, 0–28 cm soil moisture data were obtained from the monthly ERA5–Land dataset provided by the European Centre for Medium–Range Weather Forecasts (ECMWF) [37]. Publicly available datasets were analyzed in this study. These data can be found here: [https://cds.climate.copernicus.eu/], accessed on 1 October 2023.

In this study, based on the local variance method [38], regional climate change and land cover details were captured, confirming that the spatial resolution of 0.05° is better than 0.1°. Nearest–neighbor interpolation was used for resampling with the Terra package in R [39], preserving original values without smoothing artifacts, suitable for categorical climate data. A sensitivity analysis compared the effects of changing resolution from 0.1° to 0.05°, showing variations within ±0.02 and no significant impact on conclusions. Missing values were replaced with the mean of respective variables using mean imputation. Additional tests confirmed no significant errors (error < 1%). Data sources and variables are summarized in Table 1.

Table 1. Summary of data used in this study.

Data Type	Data Name	Unit	Spatial Resolution	Temporal Resolution	Spatial Range	Source
Climate data	Precipitation	mm	0.1°	daily	Global	MSWEP
	Temperature	°C	0.1°	daily	Global	MSWX
	Solar radiation	W m^{-2}	0.1°	daily	Global	MSWX
	Air pressure	Pa	0.1°	monthly	Global	MSWX
	Relative humidity	%	0.1°	monthly	Global	MSWX
	Soil moisture	%	0.1°	monthly	Global	ERA5–Land
Plant productivity	kNDVI	–	0.05°	monthly	Global	MOD13C2
Land cover	Land cover	–	0.05°	yearly	Global	MCD12C1

2.3. Land Cover Changes

The dynamics of land cover changes in the APENC region were systematically analyzed. First, the areal percentage of each land cover type was calculated annually from 2001 to 2022, and trends were evaluated using linear regression. Subsequently, the specific transitions among land cover types were analyzed, categorizing these changes by type. Finally, the Mann–Kendall (MK) test [40,41] was applied to assess the statistical significance of the changes within the same categories of land cover.

2.4. Influence of Land Cover Variations on Vegetation's Climatic Sensitivity

To explore whether land cover change impacts the sensitivity of climate change to local vegetation productivity, we performed linear mixed-effects models in land cover change regions and moderation effects in APENC. In linear mixed-effects models, mean kNDVI in growing season is the dependent variable, and climatic variables (i.e., growing-season precipitation amount, VPD, interaction between growing season precipitation amount and land cover and interaction between growing season VPD and land cover) are independent variables, with long-term land cover series as random factor.

Furthermore, the relationship between vegetation indices and climate factors across different land cover types was explored in APENC. The moderating effect of land cover on the relationship between climate factors and vegetation productivity was assessed through group regression analysis, utilizing the R package "bruceR". In this analysis, land cover type was treated as the moderating variable and categorized into distinct land cover types. Vegetation indices were considered as the dependent variable, while precipitation and VPD were regarded as independent variables.

2.5. Sensitivities of Vegetation Index to Climate Change

A systematic analysis was conducted to evaluate the relationships between these variables. First, Pearson correlation coefficients were calculated to assess the pairwise relationships between all climate variables [42]. This step provided initial insight into the strength and direction of inter-variable dependencies, highlighting the potential presence of multicollinearity. The correlation matrix revealed significant correlations among some precipitation metrics and other climatic factors, suggesting the need for further diagnostic measures [43]. Next, the Variance Inflation Factor (VIF) was computed for each independent variable to quantify multicollinearity in the dataset. VIF values exceeding the commonly accepted threshold of 5 indicated substantial multicollinearity among certain variables, particularly within precipitation metrics [44]. These results further justified the use of ridge regression to ensure the robustness of the analysis.

To address multicollinearity among key climatic variables—such as precipitation amount, dry-day fraction, precipitation intensity, and VPD—ridge regression analysis was utilized to evaluate the sensitivity of the vegetation index to climate factors. Ridge regression effectively mitigates multicollinearity, providing a robust analytical framework for understanding complex inter-variable relationships [2].

In the ridge regression model, the average of kernel Normalized Difference Vegetation Index (kNDVI) in growing season was treated as the dependent variable. Independent variables included growing−season temperature, precipitation amount, precipitation intensity, precipitation frequency, dry−day fraction, radiation, and VPD, as well as pre-season temperature and precipitation amount. Prior to analysis, all variables were normalized to a 0–1 range to ensure consistency.

The regression coefficients derived from the ridge regression analysis were used to quantify the sensitivities of vegetation productivity to climatic changes, providing valuable insights into how vegetation responds to various climatic drivers.

2.6. Spatial Autocorrelation Analysis

Spatial autocorrelation analysis is a method used to determine whether there is spatial aggregation or clustering of a geographic phenomenon or variable by examining its overall degree of spatial dispersion [45]. This analysis reveals whether there is a correlation between the values of attributes of geographic elements and their neighboring elements, providing insights into the spatial distribution patterns of the phenomenon under investigation.

In this study, two main indices were used to assess spatial autocorrelation: the Global Moran's I Index and the Local Moran's I Index.

The Global Moran's I Index is a measure of the overall spatial autocorrelation of a variable across the entire study area. It quantifies the degree of similarity or dissimilarity of values of a variable in neighboring locations. The formula for calculating the Global Moran's I is as follows:

$$Global\ Moran's\ I = \frac{n\sum_{i=1}^{n}\sum_{j=1}^{n}\omega_{ij}(x_i - \bar{x})(x_j - \bar{x})}{\sum_{i=1}^{n}(x_i - \bar{x})^2} \tag{1}$$

where n indicates number of spatial units (e.g., pixels); xi and xj indicate values of the attribute at locations; $\bar{x}$ indicates mean value of the attribute across all locations; ω_{ij} indicates spatial weight between locations *i* and *j*.

The Local Moran's I Index measures the degree of spatial autocorrelation at each individual location, allowing for the identification of local patterns of spatial clustering. It helps to determine whether certain areas are characterized by significant spatial clusters or outliers of high or low values, which may not be evident in the global analysis. The formula for the Local Moran's I at location iii is given by the following:

$$Local\ Moran's\ I = \frac{n(x_i - x)\sum_{j=1}^{n} \omega_{ij}(x_j - \bar{x})}{\sum_{i=1}^{n}(x_i - \bar{x})^2} \qquad (2)$$

where n indicates number of spatial units (e.g., pixels); xi and xj indicate values of the attribute at locations; $\bar{x}$ indicates mean value of the attribute across all locations; ω_{ij} indicates spatial weight between locations *i* and *j*.

3. Results

3.1. Spatial–Temporal Processes of Land Cover Changes

An analysis of the MCD12C1 dataset revealed that approximately 17% of the APENC region experienced land cover changes between 2001 and 2022, with notable alterations occurring in grasslands and croplands (Figure 2). Specifically, the proportion of grasslands in the region declined significantly at an annual rate of 0.34% ($y = -0.0034x + 7.72$, $p < 0.05$, $R^2 = 0.78$), while the percentage of croplands increased significantly by approximately 0.26% per year ($y = 0.0026x - 5.09$, $p < 0.05$, $R^2 = 0.79$) (Figure 2a). In contrast, the areal percentages of forests, shrublands, and barren lands exhibited little variation throughout the study period.
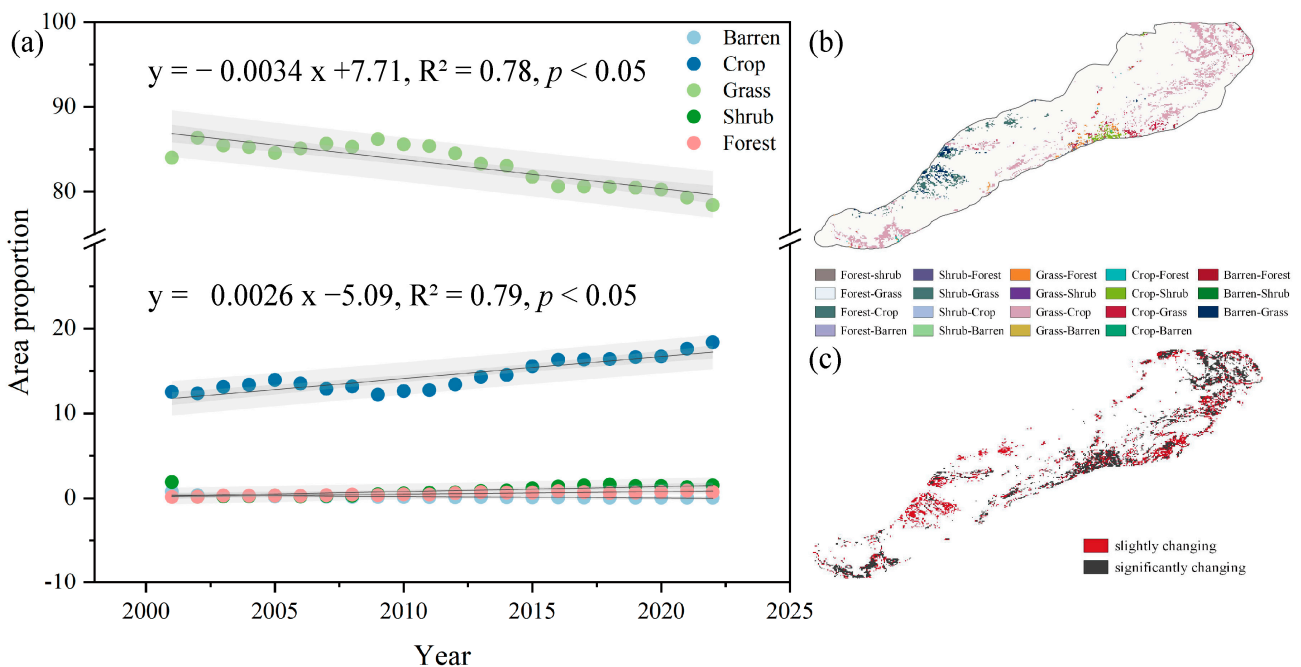

Figure 2. Land use and land cover change in the APENC from 2001 to 2022. (**a**) Trend of land use and land cover changes in the APENC region from 2001 to 2022; (**b**) the map illustrates the specific transitions of land cover types between 2001 and 2022; (**c**) the spatial distribution of land cover change significance was determined using the Mann–Kendall (MK) test. White areas indicate no significant changes in land cover, and red areas represent regions with slight changes ($-1.96 < z < 1.96$), while black areas denote regions with significant land cover changes ($z > 1.96$ or $z < -1.96$).

The predominant transitions were observed between grasslands and croplands, with conversions from grasslands to croplands accounting for 43.6% of all changes, while transitions from croplands to grasslands represented 26.2% (Figure 2b).

The significance of land cover changes was analyzed using the Mann–Kendall (MK) test. The results indicated that regions with significant changes in land cover, denoted by black, accounted for 53.7% of the total change area (with z > 1.96 or z < −1.96), suggesting that these areas experienced substantial alterations in land cover. In contrast, regions with non-significant changes (indicated by red) occupied 46.3% of the change area, with z-values ranging between −1.96 and 1.96, suggesting that the land cover changes in these areas were either minor or not statistically significant. Additionally, the white areas represent regions with no changes. These findings suggest that the spatial distribution of land cover changes in the study area exhibits certain unevenness, with areas of significant change slightly outweighing those with non-significant changes (Figure 2c).

3.2. Impacts of Land Cover Changes on Vegetation Climatic Sensitivity

The analysis results revealed significant interactions between climate factors, specifically vapor pressure deficit (VPD) and precipitation, and land cover, highlighting their collective impact on vegetation productivity, as assessed by the kNDVI. Notably, VPD exhibited a significant negative sensitivity to the kNDVI in 12.54% of the region ($p < 0.05$), indicating that increased atmospheric dryness detrimentally affected vegetation productivity in these areas (Figure 3a). In contrast, a positive sensitivity to VPD was observed in 6.32% of the region ($p < 0.05$), suggesting that moderate increases in VPD might have benefited vegetation in certain ecosystems. When the interaction between VPD and land cover was accounted for, the significant negative sensitivity was reduced by 5.32%, and the positive sensitivity diminished by 3.28% (Figure 3b). This reduction underscored the role of land cover in moderating vegetation responses to VPD, likely attributed to variations in vegetation types, land management practices, or adaptive characteristics.

Similarly, precipitation demonstrated a significant positive sensitivity to the kNDVI in 10.54% of the region ($p < 0.05$), indicating that increased precipitation positively influenced vegetation productivity in these areas (Figure 3c). Conversely, negative sensitivity was noted in 5.64% of the region ($p < 0.05$), suggesting that excessive rainfall may have detrimental effects on vegetation due to factors such as waterlogging or nutrient leaching. When considering the interaction between precipitation and land cover, the positive sensitivity decreased substantially by 8.57%, while the negative sensitivity saw a slight reduction of 1.39% (Figure 3d). These findings emphasized the influence of land cover in modulating precipitation's effects on vegetation productivity, potentially through variations in water retention capacity, soil properties, or vegetation structure.

The interaction terms further indicated that land cover played a pivotal role in shaping vegetation responses to climate variables. Incorporating these interactions into the model enhanced the understanding of the spatially heterogeneous impacts of climate factors on vegetation dynamics, providing a more comprehensive view of the underlying ecological processes.

In this study, the response of the vegetation index (kNDVI) to climate factors (precipitation and VPD) was analyzed by using the land cover type as a moderating variable. The results showed that the introduction of the land cover type significantly improved the fitting accuracy of the regression model. Specifically, the regression model coefficient of determination (R^2) between the kNDVI and precipitation was 0.75 when the land cover type was not considered, whereas the R^2 of the model was improved to 0.81 when the land cover type was added as a moderating effect. Similarly, the R^2 of the regression model between the kNDVI and VPD was improved from 0.72 to 0.76, This further confirmed the significant role of land cover type in moderating and influencing the vegetation response.
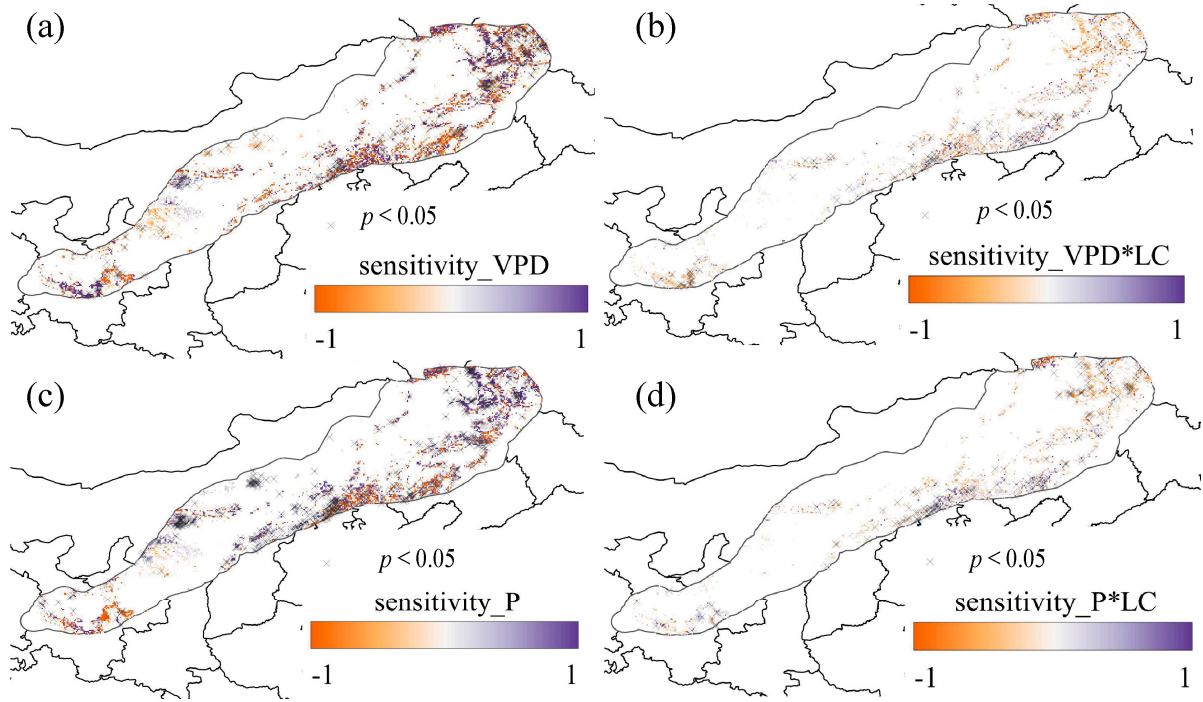
Figure 3. Results of the raster-scale linear mixed-effects model, with land cover as a random effect and climate factors as fixed effects. (**a**) illustrates the impact of vapor pressure deficit (VPD) on the vegetation index (kNDVI). (**b**) highlights the interaction between VPD and land cover. (**c**) shows the impact of precipitation on the vegetation index (kNDVI). (**d**) depicts the interaction between precipitation and land cover. Regions labeled with black × indicate statistically significant trends ($p < 0.05$).

There were significant differences in the response of the kNDVI to precipitation and VPD under different land cover types. With the increase in precipitation, there was a significant positive correlation ($p < 0.001$) between the kNDVI and precipitation in crop and grass, while the response was weaker or even close to zero in forest, shrub, and barren areas (Figure 4a). Unlike the response trend of precipitation, the kNDVI of grass and crop showed a significant negative correlation with VPD as VPD increased; however, the kNDVI of forested areas showed a positive correlation with VPD (Figure 4b). The kNDVI of shrub and barren areas showed little response to changes in VPD. Therefore, the role of the land cover type in regulating the response of vegetation to climate factors cannot be ignored.
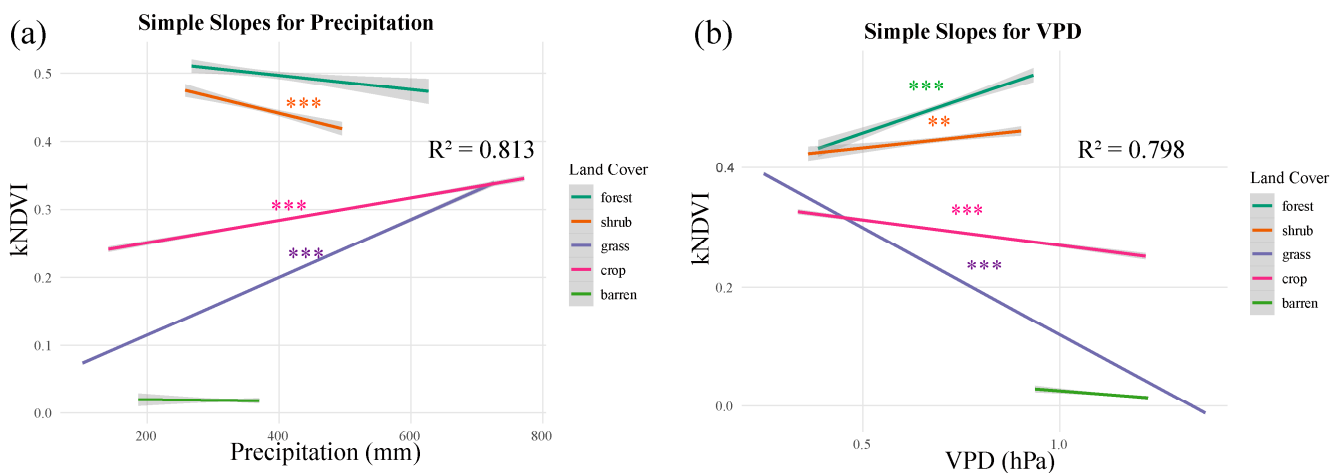

Figure 4. The effect of precipitation on kNDVI across different land cover types (**a**) and the effect of VPD on kNDVI across different land cover types (**b**). The length of each line represents the range of

the climatic factor (i.e., the difference between its maximum and minimum values) for the respective land cover type. The slope of the line indicates the strength and direction of the relationship: lines in the first and third quadrants represent a positive correlation between the climatic factor and kNDVI, whereas lines in the second and fourth quadrants indicate a negative correlation. ** indicates $p < 0.01$; *** indicates $p < 0.001$.

3.3. Correlation Among Climate Factors and Collinearity Analysis

The correlation matrix revealed significant relationships among various climatic factors, highlighting their complex interdependencies. Strong positive correlations were observed between soil water variability (SWV) and precipitation (P) ($r = 0.85$, $p < 0.001$), as well as between vapor pressure deficit (VPD) and radiation (Rad) ($r = 0.78$, $p < 0.001$) (Figure 5). Conversely, strong negative correlations exist between growing-season VPD and precipitation ($r = -0.80$, $p < 0.001$), as well as between radiation (Rad) and precipitation (P) ($r = -0.74$, $p < 0.001$) (Figure 5).
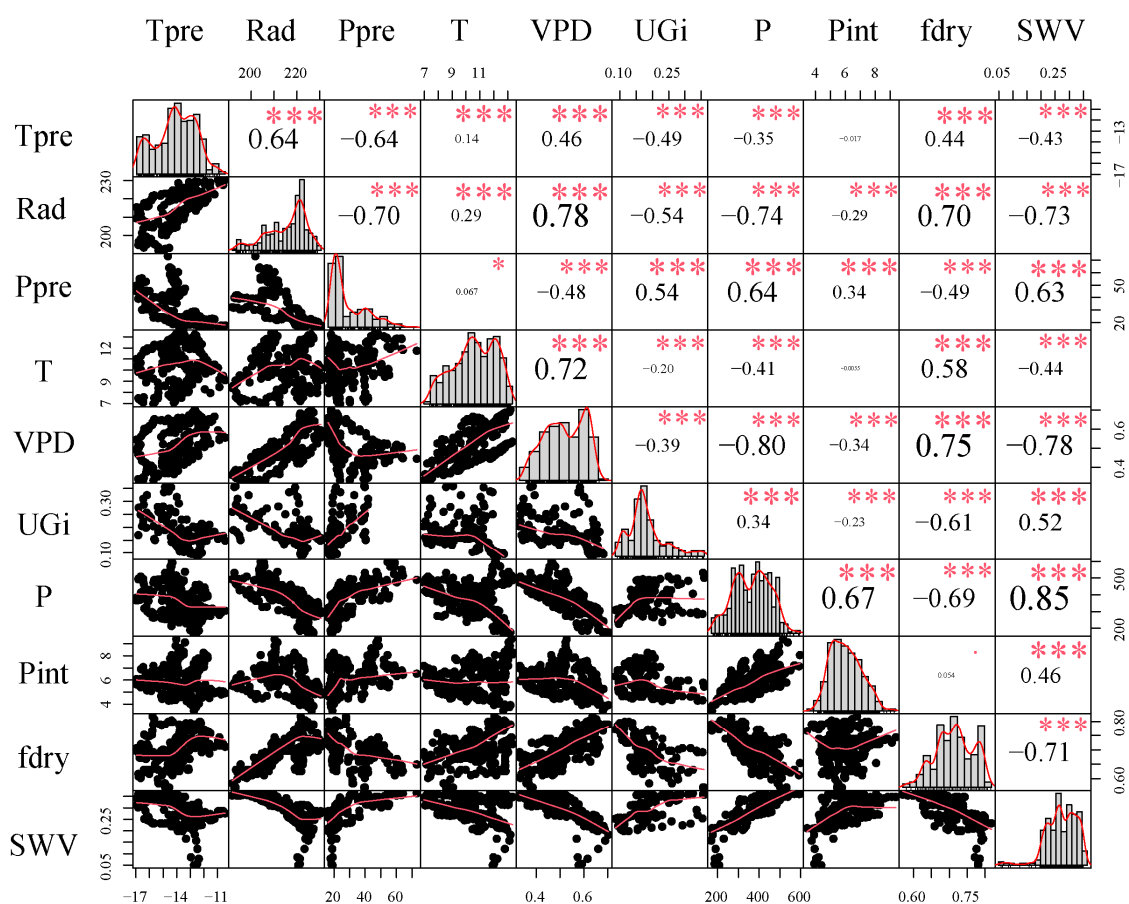

Figure 5. Pearson correlation coefficients among climate variables. The diagonal displays histograms of each variable's distribution, while scatterplots show the distribution trends and linear correlations between variables, with red curves representing nonlinear fitting trends. The correlation coefficients shown are Pearson coefficients, and the significance levels are indicated with asterisks (* for $p < 0.05$, and *** for $p < 0.001$).

The significant correlations among variables pointed to the presence of multicollinearity, which could compromise the reliability of regression analyses. To quantify the degree of multicollinearity, the Variance Inflation Factor (VIF) was calculated, with the results presented in Table 2. The VIF analysis confirmed the existence of substantial multicollinearity among climatic variables. Consequently, ridge regression was employed as a robust statistical method to address this issue and mitigate the effects of multicollinearity in subsequent analyses.

Table 2. Variance Inflation Factor of climate factor.

	P	fdry	Pint	VPD	T	Rad	SWV	Tpre	Ppre	UGi
VIF	38.3	28.1	18.5	13.2	9.1	8.7	5.3	3.9	2.8	2.3

3.4. Spatial Distributions of Sensitivities of Vegetation Index to Climate Variability

Subsequently, ridge regression was employed to assess the sensitivities of vegetation productivity to climate change across the entire APENC region. All sensitivity values noted below represent averages calculated for the entire region. The modeling results of the ridge regression model used in this study can be expressed as follows: kNDVI = 5.1218 + 0.125Ppre + 0.090P + 0.086Pint + 0.061Tpre + 0.056SWV + 0.019T + 0.0039UGi−0.046fdry − 0.0584Rad− 0.117VPD. The model with R^2 = 0.891 and RMSE = 0.0125. The results revealed that both pre-season precipitation and temperature, along with growing-season precipitation, soil moisture, and precipitation intensity, had a positive effect on vegetation productivity. Conversely, VPD, radiation, and the dry-day fraction exhibited negative impacts on vegetation productivity (Figure 6). Notably, pre-season precipitation showed the highest positive sensitivity, while VPD demonstrated the greatest negative sensitivity (Figure 6). Additionally, the influence of growing-season temperature and precipitation frequency (i.e., UGi) on vegetation productivity was minimal (Figure 6).
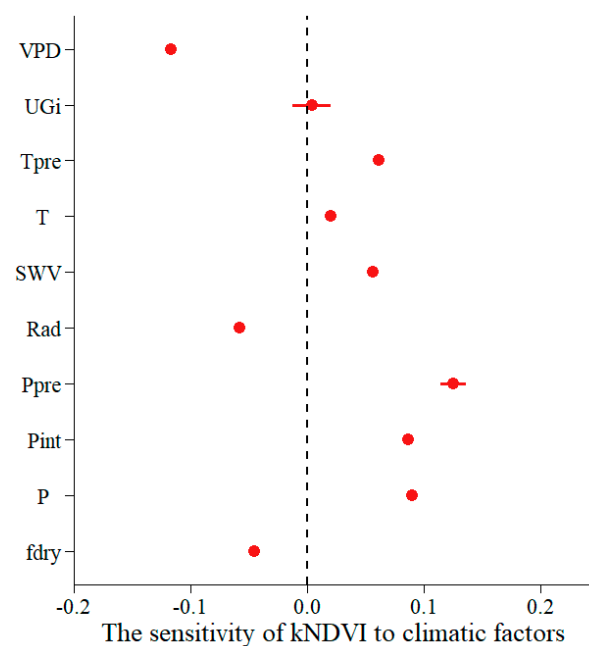

Figure 6. The sensitivity of mean kNDVI in growing season to intra-season climatic factors used the ridge regression in APENC from 2001 to 2022. Notes: VPD indicates vapor pressure deficit (hPa), UGi indicates Unranked−Gini index (no unit), Tpre indicates pre−season temperature (°C), T indicates temperature (°C), SWV indicates soil moisture (%), Rad indicates radiation (W/m^2), Ppre indicates pre-season precipitation amount (mm), Pint indicates precipitation intensity (mm/day), P indicates precipitation amount (mm), and fdry indicates dry−day fraction (%). The error bars represent the 95% confidence intervals of the sensitivity estimates, reflecting the degree of uncertainty associated with the regression coefficients for each climatic factor.

From a spatial perspective, significant positive sensitivity to growing-season precipitation was observed in 34.12% of the APENC region, followed by 23.43% for growing-season SWV, 22.93% for pre-season precipitation, and 7.89% for pre-season temperature (Figure 7b,c,f,h, Table 3). In contrast, 38.80% of the region exhibited significant negative sensitivity to VPD, with 13.72% for the dry-day fraction and 9.73% for radiation (Figure 7a,e,j,

Table 3). Furthermore, no significant differences in climatic sensitivity were observed across biome types (i.e., forests, shrublands, grasslands, croplands and barren) within the APENC region (Figure 8).
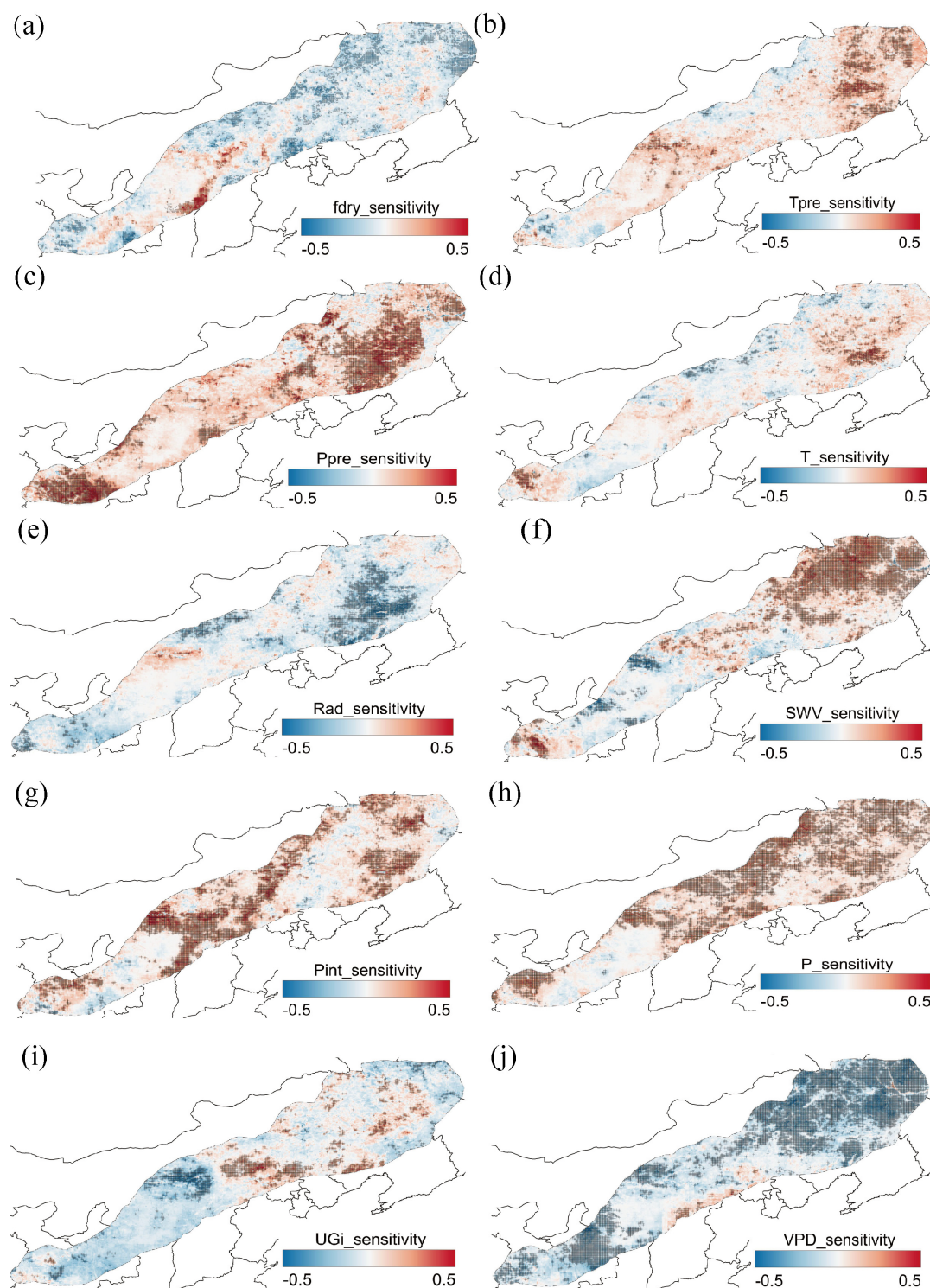

Figure 7. Spatial distribution of the sensitivity between mean kNDVI in growing season and intra-season climatic factors in APENC from 2001 to 2022. a–i show the sensitivity of dry-day fraction (%) (**a**), pre−season temperature (°C) (**b**), pre−season precipitation (mm) (**c**), temperature (°C) (**d**), radiation(W/m^2) (**e**), soil moisture (%) (**f**), precipitation intensity (mm/day) (**g**), precipitation (mm) (**h**), Unranked−Gini index (no unit) (**i**), and vapor pressure deficit (hPa) (**j**), respectively. Regions labeled with black dots indicate statistically significant trends ($p < 0.05$).

Table 3. The pixel proportion of the sensitivity between kNDVI and climatic factors.

|	Positive (Not Significant)	Positive (Significant)	Negative (Not Significant)	Negative (Significant)
Fdry (dry-day fraction)	28.4%	2.36%	55.52%	13.72%
Tpre (pre-season temperature)	70.89%	7.89%	20.71%	0.51%
Ppre (pre-season precipitation)	67.95%	22.93%	8.99%	0.13%
T (temperature)	55.61%	2.94%	40.15%	1.30%
Rad (radiation)	26.16%	0.19%	63.92%	9.73%
SWV (soil moisture)	45.04%	23.43%	29.07%	2.46%
Pint (precipitation intensity)	58.23%	22.56%	18.59%	0.62%
P (precipitation)	55.41%	34.12%	10.38%	0.09%
Ugi (Unranked-Gini index)	43.25%	5.75%	47.60%	3.40%
VPD (vapor pressure deficit)	7.34%	0.47%	53.39%	38.80%
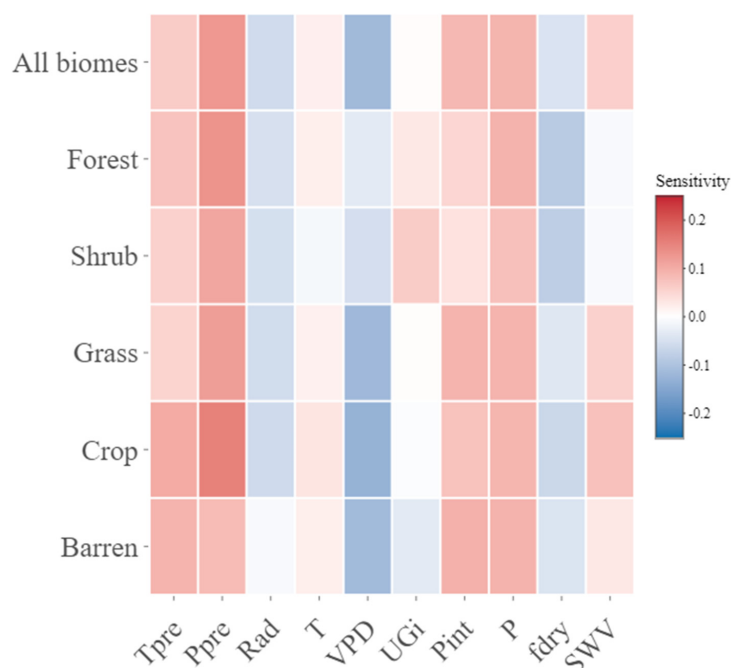
Figure 8. Sensitivity of mean kNDVI in growing season to intra-season climatic variables across different biomes. Notes: Tpre indicates pre−season temperature (°C), Ppre indicates pre−season precipitation amount (mm), Rad indicates radiation (W/m^2), T indicates temperature (°C), VPD indicates vapor pressure deficit (hPa), UGi indicates Unranked−Gini index (no unit), Pint indicates precipitation intensity (mm/day), P indicates precipitation amount (mm), fdry indicates dry−day fraction (%), and SWV indicates soil moisture (%).

3.5. Spatial Autocorrelation Analysis Results

The sensitivity of vegetation to climatic factors exhibited significant spatial heterogeneity. The global Moran's I values indicated strong spatial autocorrelations for all climatic factors, suggesting that regions with similar sensitivities were spatially clustered rather than randomly distributed (Table 4). Pre−season precipitation (Ppre), precipitation intensity (Pint), and growing season precipitation (P) had strong and concentrated effects on vegetation indices, indicating a significant and consistent vegetation response to these climatic factors (Figure 9). In contrast, the Unranked−Gini index (UGi) and radiation (Rad) exhibited weaker and more dispersed effects on vegetation indices, suggesting limited vegetation sensitivity to these variables (Figure 9). These findings underscored the significant spatial clustering of vegetation sensitivity to climatic factors, highlighting the importance of fine-scale spatial modeling in better understanding vegetation dynamics under climate change.

Table 4. Global Moran's I Index and significance testing for vegetation sensitivity to climatic factors.

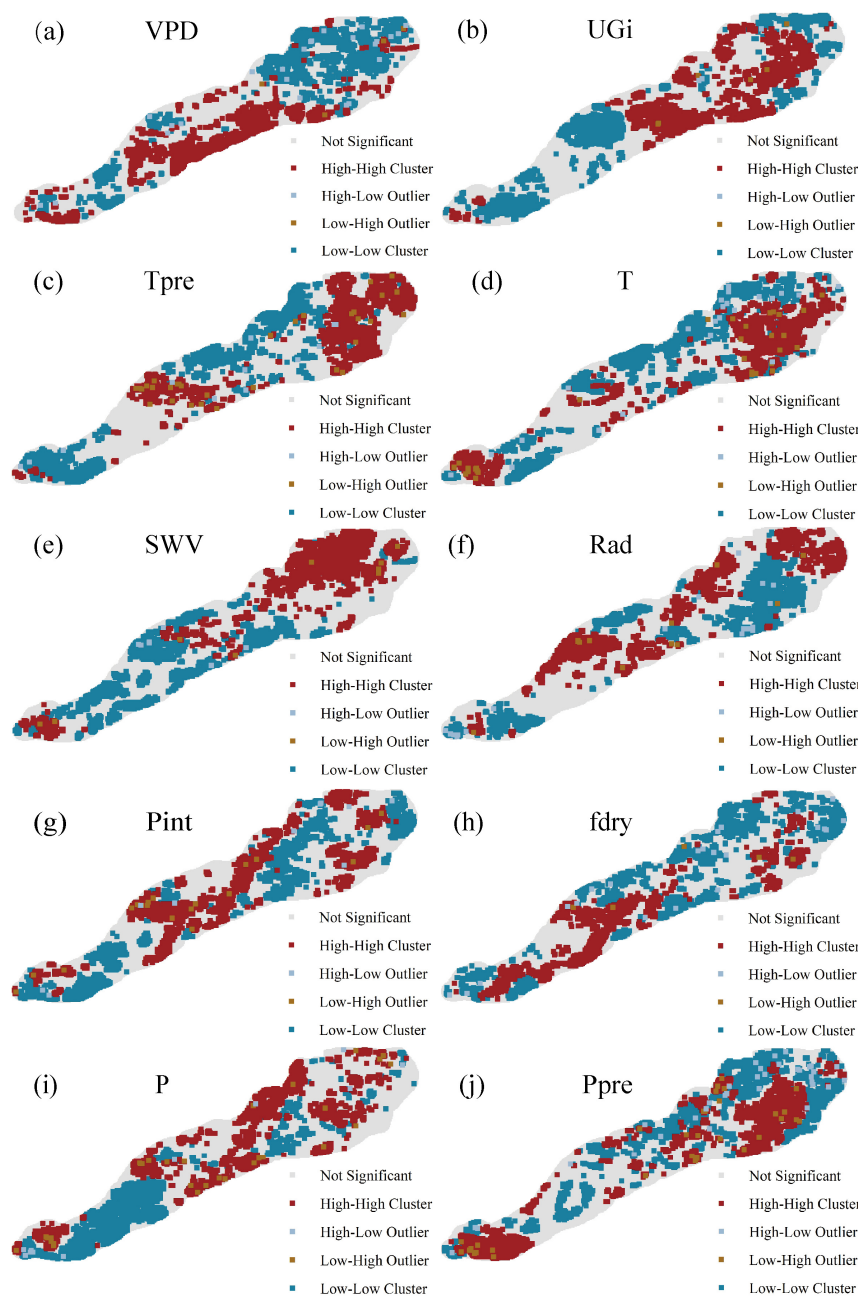|	fdry	P	Ppre	Pint	Rad	SWV	T	UGi	VPD	Tpre
Moran's I	0.84	0.85	0.86	0.88	0.88	0.89	0.84	0.89	0.86	0.86
Z	162.53	163.21	164.79	168.84	168.99	171.30	159.99	170.22	165.54	164.65
P	<0.01	<0.01	<0.01	<0.01	<0.01	<0.01	<0.01	<0.01	<0.01	<0.01

Figure 9. Spatial distribution of clustering and outlier patterns for vegetation sensitivity to climatic variables. High−High clusters (red) and Low−Low clusters (blue) indicate regions with significant spatial autocorrelation, while High−Low (brown) and Low−High (light blue) outliers represent localized deviations. Non−significant areas (gray) lack strong clustering patterns. Variables include (**a**) vapor pressure deficit (VPD), (**b**) Unranked−Gini index (UGi), (**c**) pre−season temperature (Tpre), (**d**) growing−season temperature (T), (**e**) soil moisture (SWV), (**f**) radiation (Rad), (**g**) growing−season precipitation (Pint), (**h**) dry−day fraction (fdry), (**i**) precipitation amount (P), and (**j**) pre−season precipitation (Ppre).

4. Discussion

4.1. Relationship Between LUCC and Anthropogenic Activities

LUCC was predominantly driven by anthropogenic activities [46,47]. This study observed that 17% of the land cover in the APENC region changed between 2001 and 2022, with approximately 69.8% of these changes resulting from transitions between croplands and grasslands. This finding aligned with prior research Wei et al. [6]. The predominance of cropland-to-grassland transitions suggested a continuous cycle of land management practices, such as cropland abandonment, which might have exacerbated habitat fragmentation and ecosystem instability [48]. Understanding the mechanisms underlying these transitions was essential for designing effective conservation strategies to mitigate the negative ecological impacts of land use changes [49].

The dynamics of land use in the APENC from 2005 to 2009 were primarily influenced by policy interventions and population migration. During this period, cropland areas declined while grasslands expanded, driven by two major factors. First, the "Grain for Green" initiative led to the conversion of sandy and low-quality croplands into ecologically restored land [50]. Second, rural population declines, largely due to urban migration, resulted in a shortage of agricultural labor. Consequently, large areas of cropland were abandoned, facilitating grassland expansion [6]. Official statistics indicate that the agricultural population decreased from 745 million in 2005 to 689 million in 2009, reflecting substantial demographic shifts. In underdeveloped rural areas, agricultural systems proved particularly vulnerable to changes in labor availability, climatic conditions, and policy measures.

In contrast to the 2005–2009 period, the years from 2009 to 2022 witnessed a reversal, with grasslands increasingly converted into croplands. This shift could be attributed to two key factors. First, the abolition of the agricultural tax in 2006 curbed cropland reduction. Second, the 2009 introduction of the "Defend the Cropland Red Line" policy mandated that cropland area be maintained above 1.2 million square kilometers to safeguard national food security [51]. These trends reflected broader land use shifts characterized by intensified agricultural practices and land conversion. Such changes posed significant challenges for balancing ecological conservation with human demands [52].

Grassland degradation remained a pressing environmental issue. Between 2001 and 2022, grasslands declined at an annual rate of 0.34%. This persistent decline was concerning given the critical ecological roles of grasslands, including carbon sequestration, soil stabilization, and the provision of habitats for diverse species [53]. Continued degradation could have compromised ecosystem resilience, resulting in soil erosion, degradation, and biodiversity loss [54,55]. It was, therefore, imperative to prioritize grassland conservation and restoration efforts to ensure ecosystem stability.

In addition to LUCC, other environmental and ecological factors could also contribute significantly to vegetation resilience [56]. Soil properties, such as soil organic matter content, texture, and water retention capacity, played critical roles in supporting vegetation by regulating water and nutrient availability [57]. Moreover, biodiversity, including species richness and functional diversity, enhanced ecosystem stability and resilience by promoting complementary resource use and reducing susceptibility to disturbances [58]. These factors, alongside LUCC, interacted in complex ways to shape vegetation dynamics and resilience. Therefore, a more comprehensive framework is needed in the future that integrated LUCC with soil properties and biodiversity to better understand and manage vegetation resilience in the APENC region.

4.2. Impacts of Land Cover Changes on Vegetation Sensitivity to Climate

The sensitivity of vegetation to climate change varied significantly across different land cover types in the study area. This study revealed that the relationships between

precipitation, VPD, and the kNDVI differed markedly across various land cover types. Specifically, precipitation is strongly positively correlated with the kNDVI in grasslands and croplands, a result consistent with Liu et al. [59], indicating that water supply was crucial for vegetation growth in these ecosystems. Increased precipitation effectively enhanced soil moisture, thereby stimulating metabolic processes such as photosynthesis and nutrient absorption in grasslands and croplands [60]. In contrast, the relationship between precipitation and the kNDVI is weaker in forests and shrub, which aligned with the findings of Jia et al. [27]. This might have been due to the typically deeper root systems and larger canopy sizes of woody plants. The deeper root systems allowed for better access to soil moisture, while the larger canopy sizes helped reduce fluctuations in the kNDVI, thus diminishing the sensitivity of vegetation to variable precipitation.

Regarding VPD, the kNDVI in grasslands and croplands showed a negative correlation with VPD, consistent with the findings of Liu et al. [59], suggesting that higher VPD decreased relative humidity, exacerbating water loss in grassland plants. Under water stress conditions, grassland plants typically restricted stomatal opening to reduce water loss [61], which limits photosynthesis and suppressed vegetation growth [62]. However, in forests, VPD is positively correlated with the kNDVI, possibly indicating a higher adaptive capacity of forests under drought conditions. Flach et al. [63] suggested that, globally, forests were less sensitive to drought than other vegetation types. In summary, the results of this study highlighted the critical role of land cover type in moderating climate change impacts, particularly in terms of the differential responses of vegetation to precipitation and VPD.

Due to the impact of LUCC on the sensitivity of vegetation productivity to climate change, the ongoing intensification of global climate change presented significant challenges to regional management in the APENC [64]. Therefore, it was crucial to implement effective measures to enhance the ecological resilience of the region [9,65]. For instance, in drought years that induced by pre-seasonal precipitation deficiency, it was suggested that, on the one hand, the proportion of agriculture should be reduced and animal husbandry increased; on the other hand, water resource regulation along with irrigation technologies (e.g., drip irrigation and micro-sprinkler systems, etc.) should be adopted to reduce water stress. Moreover, the implementation of precipitation harvesting and storage systems could have been a viable strategy during dry season. Conversely, when pre-seasonal precipitation is relatively abundant, it might have been beneficial to increase the area of crops, particularly by introducing drought-resistant crops such as wheat and potatoes [10]. This strategy would have helped to minimize the negative impacts of climate change and reduce the potential risk of a food crisis [66].

4.3. Vegetation Index Response to Climate Change

Pre-season precipitation played a pivotal role in determining vegetation growth, with findings highlighting its greater impact on vegetation productivity compared to growing-season precipitation. This difference was likely due to the critical role of snowfall in water storage. Increased snowfall enhanced water reserves, which subsequently promoted vegetation growth and improved vegetation indices [17–19]. These findings aligned with earlier studies of Barrett et al. [67] that emphasized the importance of adequate water availability for plant growth, particularly in semi-arid and arid regions such as the APENC.

Warmer pre-season temperatures accelerated snowmelt, leading to enhanced soil water storage before the growing season began. The analysis demonstrated that pre-season temperatures exerted a stronger influence on vegetation productivity than growing-season temperatures. This outcome was likely a consequence of rising pre-season temperatures altering precipitation patterns, shifting precipitation from snow to rain [67,68]. The resulting

early snowmelt increased soil moisture storage during critical periods when plants were most sensitive to moisture deficits [20]. These conditions established favorable water availability well in advance of the growing season. Conversely, growing-season precipitation and temperatures had comparatively limited effects as plants were already in their active growth phase and are more responsive to immediate water availability.

Precipitation patterns, including both amount and intensity, had positive effects on vegetation productivity in arid regions. Increased precipitation alleviated water stress, enhancing physiological processes such as photosynthesis and reducing water limitations on growth [69]. For example, Wang et al. [65] pointed out that precipitation was a key factor influencing vegetation productivity, particularly in arid and semi-arid regions. Furthermore, single large rainfall events had been shown to result in greater productivity gains compared to multiple smaller events of equivalent total precipitation, particularly in grassland ecosystems [69]. Conversely, light precipitation events below 5 mm often had negligible effects on vegetation indices, as observed in grasslands across northern China [70].

In contrast, vapor pressure deficit (VPD) and dry-day fraction exerted negative impacts on vegetation productivity, highlighting potential vulnerabilities. Elevated VPD reduced humidity and increased evaporative stress, which impaired photosynthesis and transpiration, thereby diminishing productivity [71]. Similarly, prolonged periods of drought, reflected in an increased dry-day fraction, exacerbated water stress by limiting stomatal conductance and reducing carbon uptake [72]. These findings underscored the importance of effective water resource management, particularly given the growing aridity associated with climate change [73]. Despite these challenges, vegetation in the APENC region exhibited adaptive mechanisms to cope with increasing VPD and prolonged droughts. For instance, plants may have reduced stomatal conductance to minimize water loss under high evaporative demand, enhancing water-use efficiency even at the cost of reduced carbon uptake [74]. Additionally, deeper root systems enabled certain species to access groundwater during droughts [75]. At the community level, shifts in species composition favored drought-tolerant plants with traits such as high water use efficiency or drought-deciduous behavior further enhancing ecosystem resilience [76]. Mutualistic relationships, such as those with mycorrhizal fungi, also played a role in improving water and nutrient acquisition under stress [77].

These adaptive strategies not only demonstrate the resilience of vegetation in the APENC region but also emphasize the need for active management to support these natural responses. Policies promoting ecosystem restoration and the conservation of drought-adapted species are essential for mitigating the long-term impacts of climate change [78]. Looking ahead, future research should integrate climate models and land-use projections to predict how vegetation productivity may evolve under different climate scenarios and land management strategies [79]. Such projections would provide a more comprehensive understanding of the potential vulnerabilities and resilience of ecosystems, facilitating the design of adaptive management strategies that ensure ecological sustainability in the face of climate change [80]. Additionally, including socio-economic factors such as population growth, urbanization, and land policy changes would help to better capture the complexities of land-use dynamics and their interaction with climate variables.

4.4. Study Limitations

In this study, climate data with an original spatial resolution of 0.1° was resampled to 0.05° to match the resolution of land cover datasets. While resampling facilitated data integration, it introduced limitations that might have affected accuracy and reliability. Resampling did not enhance the intrinsic spatial precision of the original data; therefore, localized climate patterns, particularly in heterogeneous regions such as mountainous, might

not have been adequately represented [81]. This could have led to oversimplified analyses of relationships between climate and land surface processes as interpolation-derived finer resolutions could not fully capture small-scale variability. For example, extreme rainfall events, critical for understanding vegetation responses and hydrological processes, might have been masked [82]. Future studies should prioritize climate datasets with higher native resolutions or use advanced downscaling methods that integrate topographic and atmospheric conditions to reduce uncertainties and better represent spatial heterogeneity [83].

This study examined LUCC in the APENC region using annual data and linear regression methods. While linear regression was useful for identifying broad trends, it had limitations in capturing the complexity of LUCC, which was a non-linear and dynamic process influenced by socio-economic, environmental, and policy factors [84]. The assumption of linearity in regression models may have oversimplified the relationships between land use change, climate variability, and ecosystem responses, potentially missing key non-linear interactions. Additionally, the use of annual data limited the temporal resolution of the analysis, potentially overlooking intra-annual fluctuations that could have been critical for understanding LUCC and vegetation sensitivity. LUCC was also influenced by socio-economic factors, such as population growth and land management practices, which were not considered in this study due to data constraints [85]. Future research could address these limitations by employing non-linear modeling, machine learning, or system dynamics approaches to better capture the complexity of LUCC processes. Higher temporal resolution data could also provide deeper insights into the dynamics of LUCC and its impact on vegetation sensitivity to climate change.

5. Conclusions

This study examined the impacts of LUCC and climatic variability on vegetation primary productivity in the APENC region from 2001 to 2022. The results revealed a significant decline in grassland areas accompanied by an increase in cropland, driven by anthropogenic activities and policy changes. The effects of precipitation and VPD on the vegetation indices varied across different land cover types. Additionally, pre-season precipitation and temperature exerted a stronger influence on vegetation productivity than growing season precipitation and temperature. In contrast, both VPD and dry-day fraction were found to negatively affect vegetation productivity. These findings emphasize the complexity of climate–vegetation interactions in fragile ecosystems like the APENC. Moving forward, sustainable land management practices and continued research are imperative to ensure the ecological and agricultural sustainability of the region.

Author Contributions: L.H. and Q.W. designed this study. Y.Z. carried out the analysis and drafted the initial manuscript. X.Z., Z.G., X.G., C.M., B.W. and L.H. provided critical insights on results interpretation and text editing. All authors have read and agreed to the published version of the manuscript.

Institutional Review Board Statement: Not applicable.

Data Availability Statement: The original datasets presented in this study are available in the article. For further inquiries, please contact the corresponding author.

Conflicts of Interest: The authors declare no conflicts of interest.

References

1. He, L.; Wang, J.; Ciais, P.; Ballantyne, A.; Yu, K.; Zhang, W.; Xiao, J.; Ritter, F.; Liu, Z.; Wang, X.; et al. Non-Symmetric Responses of Leaf Onset Date to Natural Warming and Cooling in Northern Ecosystems. *PNAS Nexus* **2023**, *2*, pgad308. [CrossRef] [PubMed]
2. He, L.; Wang, J.; Peñuelas, J.; Zohner, C.M.; Crowther, T.W.; Fu, Y.; Zhang, W.; Xiao, J.; Liu, Z.; Wang, X.; et al. Asymmetric Temperature Effect on Leaf Senescence and Its Control on Ecosystem Productivity. *PNAS Nexus* **2024**, *3*, pgae477. [CrossRef]
3. Jiao, K.; Liu, Z.; Wang, W.; Yu, K.; Mcgrath, M.J.; Xu, W. Carbon Cycle Responses to Climate Change across China's Terrestrial Ecosystem: Sensitivity and Driving Process. *Sci. Total Environ.* **2024**, *915*, 170053. [CrossRef]
4. Li, C.; Zhang, S. Disentangling the Impact of Climate Change, Human Activities, Vegetation Dynamics and Atmospheric CO_2 Concentration on Soil Water Use Efficiency in Global Karst Landscapes. *Sci. Total Environ.* **2024**, *932*, 172865. [CrossRef] [PubMed]
5. Wei, B.; Wei, J.; Jia, X.; Ye, Z.; Yu, S.; Yin, S. Spatiotemporal Patterns of Land Surface Phenology from 2001 to 2021 in the Agricultural Pastoral Ecotone of Northern China. *Sustainability* **2023**, *15*, 5830. [CrossRef]
6. Wei, B.; Xie, Y.; Jia, X.; Wang, X.; He, H.; Xue, X. Land Use/Land Cover Change and It's Impacts on Diurnal Temperature Range over the Agricultural Pastoral Ecotone of Northern China. *Land Degrad. Dev.* **2018**, *29*, 3009–3020. [CrossRef]
7. Zhang, K.; Dang, H.; Tan, S.; Cheng, X.; Zhang, Q. Change in Soil Organic Carbon Following the 'Grain-for-Green' Programme in China. *Land Degrad.* **2009**, *21*, 13–23. [CrossRef]
8. Bao, Z.; Zhang, J.; Wang, G.; Guan, T.; Jin, J.; Liu, Y.; Li, M.; Ma, T. The Sensitivity of Vegetation Cover to Climate Change in Multiple Climatic Zones Using Machine Learning Algorithms. *Ecol. Indic.* **2021**, *124*, 107443. [CrossRef]
9. Wei, B.; Bao, Y.; Yu, S.; Yin, S.; Zhang, Y. Analysis of Land Surface Temperature Variation Based on MODIS Data a Case Study of the Agricultural Pastural Ecotone of Northern China. *Int. J. Appl. Earth Obs. Geoinf.* **2021**, *100*, 102342. [CrossRef]
10. Zhu, H.; Ding, H.; Bi, R.; Hou, M. Characterizing Multiscale Effects of Climatic Factors on the Temporal Variation of Vegetation in Different Climatic Regions of China. *Theor. Appl. Climatol.* **2021**, *148*, 33–47. [CrossRef]
11. Feldman, A.F.; Feng, X.; Felton, A.J. Plant responses to changing rainfall frequency and intensity. *Nat. Rev. Earth Environ.* **2024**, *5*, 276–294. [CrossRef]
12. Xue, Y.; Zhang, B.; He, C.; Shao, R. Detecting Vegetation Variations and Main Drivers over the Agropastoral Ecotone of Northern China through the Ensemble Empirical Mode Decomposition Method. *Remote Sens.* **2019**, *11*, 1860. [CrossRef]
13. Liu, Z.; Liu, Y.; Li, Y. Anthropogenic Contributions Dominate Trends of Vegetation Cover Change over the Farming-Pastoral Ecotone of Northern China. *Ecol. Indic.* **2018**, *95*, 370–378. [CrossRef]
14. Chen, W.; Li, A.; Hu, Y.; Li, L.; Zhao, H.; Han, X.; Yang, B. Exploring the Long-Term Vegetation Dynamics of Different Ecological Zones in the Farming-Pastoral Ecotone in Northern China. *Environ. Sci. Pollut. Res.* **2021**, *28*, 27914–27932. [CrossRef]
15. He, L.; Li, Z.; Wang, X.; Xie, Y.; Ye, J. Lagged Precipitation Effect on Plant Productivity Is Influenced Collectively by Climate and Edaphic Factors in Drylands. *Sci. Total Environ.* **2021**, *755*, 142506. [CrossRef] [PubMed]
16. He, L.; Xie, Y.; Wang, J.; Zhang, J.; Si, M.; Guo, Z.; Ma, C.; Bie, Q.; Li, Z.-L.; Ye, J.-S. Precipitation Regimes Primarily Drive the Carbon Uptake in the Tibetan Plateau. *Ecol. Indic.* **2023**, *154*, 110694. [CrossRef]
17. Cai, S.; Li, Q. Snow Cover Dynamics: Impacts on Soil Moisture and Plant Growth in Temperate Ecosystems. *Mol. Soil Biol.* **2024**, *3*, 109–117. [CrossRef]
18. Wang, X.; Wang, T.; Guo, H.; Liu, D.; Zhao, Y.; Zhang, T.; Liu, Q.; Piao, S. Disentangling the Mechanisms behind Winter Snow Impact on Vegetation Activity in Northern Ecosystems. *Glob. Change Biol.* **2018**, *24*, 1651–1662. [CrossRef]
19. Yang, T.; Huang, F.; Li, Q. Spatial-temporal Variation of NDVI for Growing Season and Its Relationship with Winter Snowfall in Northern Xinjiang. *Remote Sens. Technol. Appl.* **2017**, *32*, 1132–1140. [CrossRef]
20. Huang, F.; Feng, T.; Guo, Z.; Li, L. Impact of Winter Snowfall on Vegetation Greenness in Central Asia. *Remote Sens.* **2021**, *13*, 4205. [CrossRef]
21. Liang, H.; Zhao, H.; Cheng, W.; Lu, Y.; Chen, Y.; Li, M.; Gao, M.; Fan, Q.; Xu, Z.; Li, X. Accelerating Urban Warming Effects on the Spring Phenology in Cold Cities but Decelerating in Warm Cities. *Urban For. Urban Green.* **2024**, *102*, 128585. [CrossRef]
22. Wang, Z. The Variability in Sensitivity of Vegetation Greenness to Climate Change across Eurasia. *Ecol. Indic.* **2024**, *163*, 112140. [CrossRef]
23. Jegede, S.L.; Lukman, A.F.; Alqasem, O.A.; Elwahab, M.E.A.; Ayinde, K.; Golam Kibria, B.M.; Adewinbi, H. Handling Linear Dependency in Linear Regression Models: Almost Unbiased Modified Ridge-Type Estimator. *Sci. Afr.* **2024**, *25*, e02324. [CrossRef]
24. Mermi, S.; Akkuş, Ö.; Göktaş, A.; Gündüz, N. A New Robust Ridge Parameter Estimator Having No Outlier and Ensuring Normality for Linear Regression Model. *J. Radiat. Res. Appl. Sci.* **2024**, *17*, 100788. [CrossRef]
25. Wang, Q.; Moreno-Martínez, Á.; Muñoz-Marí, J.; Campos-Taberner, M.; Camps-Valls, G. Estimation of Vegetation Traits with Kernel NDVI. *ISPRS J. Photogramm. Remote Sens.* **2023**, *195*, 408–417. [CrossRef]
26. Wei, B.; Xie, Y.; Wang, X.; Jiao, J.; He, S.; Bie, Q.; Jia, X.; Xue, X.; Duan, H. Land Cover Mapping Based on Time-series MODIS-NDVI Using a Dynamic Time Warping Approach: A Casestudy of the Agricultural Pastoral Ecotone of Northern China. *Land Degrad. Dev.* **2020**, *31*, 1050–1068. [CrossRef]

27. Jia, Q.; Gao, X.; Jiang, Z.; Li, H.; Guo, J.; Lu, X.; Yonghong Li, F. Sensitivity of Temperate Vegetation to Precipitation Is Higher in Steppes than in Deserts and Forests. *Ecol. Indic.* **2024**, *166*, 112317. [CrossRef]

28. Camps-Valls, G.; Campos-Taberner, M.; Moreno-Martínez, Á.; Walther, S.; Duveiller, G.; Cescatti, A.; Mahecha, M.D.; Muñoz-Marí, J.; García-Haro, F.J.; Guanter, L.; et al. A Unified Vegetation Index for Quantifying the Terrestrial Biosphere. *Sci. Adv.* **2021**, *7*, eabc7447. [CrossRef]

29. Huete, A.; Didan, K.; Miura, T.; Rodriguez, E.P.; Gao, X.; Ferreira, L.G. Overview of the Radiometric and Biophysical Performance of the MODIS Vegetation Indices. *Remote Sens. Environ.* **2002**, *83*, 195–213. [CrossRef]

30. Porcar-Castell, A.; Tyystjärvi, E.; Atherton, J.; Van Der Tol, C.; Flexas, J.; Pfündel, E.E.; Moreno, J.; Frankenberg, C.; Berry, J.A. Linking Chlorophyll a Fluorescence to Photosynthesis for Remote Sensing Applications: Mechanisms and Challenges. *J. Exp. Bot.* **2014**, *65*, 4065–4095. [CrossRef] [PubMed]

31. Wen, J.; Köhler, P.; Duveiller, G.; Parazoo, N.C.; Magney, T.S.; Hooker, G.; Yu, L.; Chang, C.Y.; Sun, Y. A Framework for Harmonizing Multiple Satellite Instruments to Generate a Long-Term Global High Spatial-Resolution Solar-Induced Chlorophyll Fluorescence (SIF). *Remote Sens. Environ.* **2020**, *239*, 111644. [CrossRef]

32. Sulla-Menashe, D.; Friedl, M.A. *User Guide to Collection 6 MODIS Land Cover (MCD12Q1 and MCD12C1) Product*; USGS: Reston, VA, USA, 2018.

33. Beck, H.E.; Wood, E.F.; Pan, M.; Fisher, C.K.; Miralles, D.G. MSWEP V2 Global 3-Hourly 0.1° Precipitation: Methodology and Quantitative Assessment. *Bull. Am. Meteorol. Soc.* **2019**, *3*, 473–500. [CrossRef]

34. Ritter, F.; Berkelhammer, M.; Garcia, C. Distinct Response of Gross Primary Productivity in Five Terrestrial Biomes to Precipitation Variability. *Commun. Earth Environ.* **2020**, *1*, 34. [CrossRef]

35. Beck, H.E.; Pan, M.; Dutra, E.; Miralles, D.G. Global 3-Hourly 0.1° Bias-Corrected Meteorological Data Including Near-Real-Time Updates and Forecast Ensembles. *Bull. Am. Meteorol. Soc.* **2022**, *103*, E710–E732. [CrossRef]

36. Duursma, R.A. Plantecophys—An R Package for Analysing and Modelling Leaf Gas Exchange Data. *PLoS ONE* **2015**, *10*, e0143346. [CrossRef] [PubMed]

37. Muñoz-Sabater, J.; Dutra, E.; Agustí-Panareda, A.; Albergel, C.; Arduini, G.; Balsamo, G.; Boussetta, S.; Choulga, M.; Harrigan, S.; Hersbach, H.; et al. ERA5-Land: A State-of-the-Art Global Reanalysis Dataset for Land Applications. *Earth Syst. Sci. Data* **2021**, *13*, 4349–4383. [CrossRef]

38. Ming, D.P.; Wang, Q.; Yang, J.Y. Spatial Scale of Remote Sensing Image and Selection of Optimal Spatial Resolution. *J. Remote Sens.* **2008**, *4*, 529–537. [CrossRef]

39. Franceschi, S.; Fattorini, L.; Gregoire, T.G. Exploiting Nearest-Neighbour Maps for Estimating the Variance of Sample Mean in Equal-Probability Systematic Sampling of Spatial Populations. *Spat. Stat.* **2024**, *64*, 100865. [CrossRef]

40. Mann, H.B. Nonparametric Tests Against Trend. *Econometrica* **1945**, *13*, 245–259. [CrossRef]

41. Kendall, M.G. *Rank Correlation Methods*; Charles Griffin: London, UK, 1948; p. 160.

42. Tan, X.; Zhang, L.; He, C.; Zhu, Y.; Han, Z.; Li, X. Applicability of Cosmic-Ray Neutron Sensor for Measuring Soil Moisture at the Agricultural-Pastoral Ecotone in Northwest China. *Sci. China Earth Sci.* **2020**, *63*, 1730–1744. [CrossRef]

43. Guo, X.; Arshad, M.U.; Zhao, Y.; Gong, Y.; Li, H. Effects of Climate Change and Grazing Intensity on Grassland Productivity—A Case Study of Inner Mongolia, China. *Heliyon* **2023**, *9*, e17814. [CrossRef] [PubMed]

44. Pradhan, P. Strengthening MaxEnt modelling through screening of redundant explanatory bioclimatic variables with variance inflation factor analysis. *Researcher* **2016**, *8*, 29–34. [CrossRef]

45. Chen, Y. New Approaches for Calculating Moran's Index of Spatial Autocorrelation. *PLoS ONE* **2013**, *8*, e68336. [CrossRef] [PubMed]

46. Lin, X.; Zhao, H.; Zhang, S.; He, Q.; Huete, A.; Yang, L.; Zhang, X.; Zhang, X.; Zhang, Q.; Cai, S. Grassland Irrigation and Grazing Prohibition Have Significantly Affected Vegetation and Microbial Diversity by Changing Soil Temperature and Moisture, Evidences from a 6 Years Experiment of Typical Temperate Grassland. *Agric. Ecosyst. Environ.* **2025**, *380*, 109414. [CrossRef]

47. Guo, Y.; Boughton, E.H.; Qiu, J. Interactive Effects of Land-Use Intensity, Grazing and Fire on Decomposition of Subtropical Seasonal Wetlands. *Ecol. Indic.* **2021**, *132*, 108301. [CrossRef]

48. Kong, X. Hotspots of Land-Use Change in Global Biodiversity Hotspots. *Resour. Conserv. Recycl.* **2021**, *174*, 105770. [CrossRef]

49. Li, X. Spatio-Temporal Characteristics and Driving Factors of Cultivated Land Change in Various Agricultural Regions of China: A Detailed Analysis Based on County-Level Data. *Ecol. Indic.* **2024**, *166*, 112485. [CrossRef]

50. He, Y.; Kou, W.; Chen, Y.; Lai, H.; Zhao, K. Returning Cropland to Grassland as a Potential Method for Increasing Carbon Storage in Dry-Hot Valley Areas. *Sustainability* **2024**, *16*, 4150. [CrossRef]

51. Li, S.; Li, X.; Sun, L.; Cao, G.; Fischer, G.; Tramberend, S. An Estimation of the Extent of Cropland Abandonment in Mountainous Regions of China. *Land Degrad. Dev.* **2018**, *29*, 1327–1342. [CrossRef]

52. Zhu, Y. Simulating the Dynamics of Cultivated Land Use in the Farming Regions of China: A Social-Economic-Ecological System Perspective. *J. Clean. Prod.* **2024**, *478*, 143907. [CrossRef]

53. Luxi, H.; Yong, G.; Defu, W.; Xiaojing, C.; Huimin, Z.; Jiamao, Y.; Miaomiao, G. Natural Grassland Restoration Exhibits Enhanced Carbon Sequestration and Soil Improvement Potential in Northern Sandy Grasslands of China: An Empirical Study. *Catena* **2024**, *246*, 108396. [CrossRef]

54. Yang, X.; You, L.; Hu, H.; Chen, Y. Conversion of Grassland to Cropland Altered Soil Nitrogen-Related Microbial Communities at Large Scales. *Sci. Total Environ.* **2022**, *816*, 151645. [CrossRef] [PubMed]

55. Xu, A.; Liu, J.; Guo, Z.; Wang, C.; Pan, K.; Zhang, F.; Pan, X. Soil Microbial Community Composition but Not Diversity Is Affected by Land-Use Types in the Agro-Pastoral Ecotone Undergoing Frequent Conversions between Cropland and Grassland. *Geoderma* **2021**, *401*, 115165. [CrossRef]

56. Hou, Y.; Zhang, M.; Wei, X.; Liu, S.; Li, Q.; Liu, W.; Cai, T.; Yu, E. A Comparison of Annual Streamflow Sensitivities to Vegetation Change and Climate Variability in Fourteen Large Watersheds along Climate Zones in China. *Catena* **2024**, *234*, 107571. [CrossRef]

57. Deng, G.; Jiang, H.; Zhu, S.; Wen, Y.; He, C.; Wang, X.; Sheng, L.; Guo, Y.; Cao, Y. Projecting the Response of Ecological Risk to Land Use/Land Cover Change in Ecologically Fragile Regions. *Sci. Total Environ.* **2024**, *914*, 169908. [CrossRef] [PubMed]

58. Sullivan, P.L.; Billings, S.A.; Hirmas, D.; Li, L.; Zhang, X.; Ziegler, S.; Murenbeeld, K.; Ajami, H.; Guthrie, A.; Singha, K.; et al. Embracing the Dynamic Nature of Soil Structure: A Paradigm Illuminating the Role of Life in Critical Zones of the Anthropocene. *Earth-Sci. Rev.* **2022**, *225*, 103873. [CrossRef]

59. Liu, L.; Zheng, J.; Guan, J.; Li, C.; Ma, L.; Liu, Y.; Han, W. Strong Positive Direct Impact of Soil Moisture on the Growth of Central Asian Grasslands. *Sci. Total Environ.* **2024**, *954*, 176663. [CrossRef]

60. Arca, V.; Power, S.A.; Delgado-Baquerizo, M.; Pendall, E.; Ochoa-Hueso, R. Seasonal Effects of Altered Precipitation Regimes on Ecosystem-Level CO_2 Fluxes and Their Drivers in a Grassland from Eastern Australia. *Plant Soil* **2021**, *460*, 435–451. [CrossRef]

61. Manzoni, S.; Vico, G.; Katul, G.; Fay, P.A.; Polley, W.; Palmroth, S.; Porporato, A. Optimizing Stomatal Conductance for Maximum Carbon Gain under Water Stress: A Meta-Analysis across Plant Functional Types and Climates: Optimal Leaf Gas Exchange under Water Stress. *Funct. Ecol.* **2011**, *25*, 456–467. [CrossRef]

62. Pastore, M.A.; Lee, T.D.; Hobbie, S.E.; Reich, P.B. Interactive Effects of Elevated CO2, Warming, Reduced Rainfall, and Nitrogen on Leaf Gas Exchange in Five Perennial Grassland Species. *Plant Cell Environ.* **2020**, *43*, 1862–1878. [CrossRef]

63. Flach, M.; Brenning, A.; Gans, F.; Reichstein, M.; Sippel, S.; Mahecha, M.D. Vegetation Modulates the Impact of Climate Extremes on Gross Primary Production. *Biogeosciences* **2021**, *18*, 39–53. [CrossRef]

64. Yue, Y.; Geng, L.; Li, M. The Impact of Climate Change on Aeolian Desertification: A Case of the Agro-Pastoral Ecotone in Northern China. *Sci. Total Environ.* **2023**, *859*, 160126. [CrossRef] [PubMed]

65. Wang, B.; Sun, R.; Deng, Y.; Zhu, H.; Hou, M. The Variability of Net Primary Productivityand Its Response to Climatic Changes Basedon the Methods of Spatiotemporal Decompositionin the Yellow River Basin, China. *Pol. J. Environ. Stud.* **2022**, *31*, 4229–4312. [CrossRef] [PubMed]

66. Wang, X.; Zhang, B.; Zhang, Z.; Tian, L.; Kunstmann, H.; He, C. Identifying Spatiotemporal Propagation of Droughts in the Agro-Pastoral Ecotone of Northern China with Long-Term WRF Simulations. *Agric. For. Meteorol.* **2023**, *336*, 109474. [CrossRef]

67. Barnett, T.P.; Adam, J.C.; Lettenmaier, D.P. Potential Impacts of a Warming Climate on Water Availability in Snow-Dominated Regions. *Nature* **2005**, *438*, 303–309. [CrossRef] [PubMed]

68. Changchun, X.; Yaning, C.; Weihong, L.; Yapeng, C.; Hongtao, G. Potential Impact of Climate Change on Snow Cover Area in the Tarim River Basin. *Environ. Geol.* **2008**, *53*, 1465–1474. [CrossRef]

69. Thomey, M.L.; Collins, S.L.; Vargas, R.; Johnson, J.E.; Brown, R.F.; Natvig, D.O.; Friggens, M.T. Effect of Precipitation Variability on Net Primary Production and Soil Respiration in a Chihuahuan Desert Grassland: Precipitation Variability in Desert Grassland. *Glob. Change Biol.* **2011**, *17*, 1505–1515. [CrossRef]

70. Yuan, X.; Li, L.; Chen, X.; Shi, H. Effects of Precipitation Intensity and Temperature on NDVI-Based Grass Change over Northern China during the Period from 1982 to 2011. *Remote Sens.* **2015**, *7*, 10164–10183. [CrossRef]

71. Yuan, W.; Zheng, Y.; Piao, S.; Ciais, P.; Lombardozzi, D.; Wang, Y.; Ryu, Y.; Chen, G.; Dong, W.; Hu, Z.; et al. Increased Atmospheric Vapor Pressure Deficit Reduces Global Vegetation Growth. *Sci. Adv.* **2019**, *5*, eaax1396. [CrossRef]

72. Satti, Z.; Naveed, M.; Shafeeque, M.; Li, L. Investigating the Impact of Climate Change on Trend Shifts of Vegetation Growth in Gilgit Baltistan. *Glob. Planet. Change* **2024**, *232*, 104341. [CrossRef]

73. Rosińska, W. Climate Change's Ripple Effect on Water Supply Systems and the Water-Energy Nexus—A Review. *Water Resour. Ind.* **2024**, *32*, 100266. [CrossRef]

74. Nasr Esfahani, M.; Sonnewald, U. Unlocking Dynamic Root Phenotypes for Simultaneous Enhancement of Water and Phosphorus Uptake. *Plant Physiol. Biochem.* **2024**, *207*, 108386. [CrossRef] [PubMed]

75. Kühnhammer, K.; Van Haren, J.; Kübert, A.; Bailey, K.; Dubbert, M.; Hu, J.; Ladd, S.N.; Meredith, L.K.; Werner, C.; Beyer, M. Deep Roots Mitigate Drought Impacts on Tropical Trees despite Limited Quantitative Contribution to Transpiration. *Sci. Total Environ.* **2023**, *893*, 164763. [CrossRef] [PubMed]

76. Van Der Molen, M.K.; Dolman, A.J.; Ciais, P.; Eglin, T.; Gobron, N.; Law, B.E.; Meir, P.; Peters, W.; Phillips, O.L.; Reichstein, M.; et al. Drought and Ecosystem Carbon Cycling. *Agric. For. Meteorol.* **2011**, *151*, 765–773. [CrossRef]

77. Wang, P.; Wang, Y.; Shu, B.; Liu, J.-F.; Xia, R.-X. Relationships Between Arbuscular Mycorrhizal Symbiosis and Soil Fertility Factors in Citrus Orchards Along an Altitudinal Gradient. *Pedosphere* **2015**, *25*, 160–168. [CrossRef]

78. Lei, T.; Wu, J.; Wang, J.; Shao, C.; Wang, W.; Chen, D.; Li, X. The Net Influence of Drought on Grassland Productivity over the Past 50 Years. *Sustainability* **2022**, *14*, 12374. [CrossRef]

79. Wu, S.; Guo, Z.; Askar, A.; Li, X.; Hu, Y.; Li, H.; Saria, A.E. Dynamic Land Cover and Ecosystem Service Changes in Global Coastal Deltas under Future Climate Scenarios. *Ocean. Coast. Manag.* **2024**, *258*, 107384. [CrossRef]

80. Hussien, K.; Kebede, A.; Mekuriaw, A.; Beza, S.A.; Erena, S.H. Spatiotemporal Trends of NDVI and Its Response to Climate Variability in the Abbay River Basin, Ethiopia. *Heliyon* **2023**, *9*, e14113. [CrossRef]

81. New, M.; Lister, D.; Hulme, M.; Makin, I. A High-Resolution Data Set of Surface Climate over Global Land Areas. *Clim. Res.* **2002**, *21*, 1–25. [CrossRef]

82. Breinl, K.; Di Baldassarre, G. Space-Time Disaggregation of Precipitation and Temperature across Different Climates and Spatial Scales. *J. Hydrol. Reg. Stud.* **2019**, *21*, 126–146. [CrossRef]

83. Abdollahipour, A.; Ahmadi, H.; Aminnejad, B. A Review of Downscaling Methods of Satellite-Based Precipitation Estimates. *Earth Sci. Inform.* **2022**, *15*, 1–20. [CrossRef]

84. Masteali, S.H.; Bayat, M.; Bettinger, P.; Ghorbanpour, M. Uncertainty Analysis of Linear and Non-Linear Regression Models in the Modeling of Water Quality in the Caspian Sea Basin: Application of Monte-Carlo Method. *Ecol. Indic.* **2025**, *170*, 112979. [CrossRef]

85. Wenbo, X.; Hengzhou, X.; Xiaoyan, L.; Hua, Q.; Ziyao, W. Ecosystem Services Response to Future Land Use/Cover Change (LUCC) under Multiple Scenarios: A Case Study of the Beijing-Tianjin-Hebei (BTH) Region, China. *Technol. Forecast. Soc. Change* **2024**, *205*, 123525. [CrossRef]